



Contents lists available at ScienceDirect

International Journal of Plasticity

journal homepage: www.elsevier.com/locate/ijplas



Coupled diffusion-mechanics framework for simulating hydrogen assisted deformation and failure behavior of metals

Vishal Singh ^a, Rakesh Kumar ^b, Yann Charles ^c, Dhiraj K. Mahajan ^{a,*}

^a Ropar Mechanics of Materials Laboratory, Department of Mechanical Engineering, Indian Institute of Technology Ropar, Rupnagar, Punjab, 140001, India

^b Department of Mechanical Engineering, Imperial College London, London, SW7 2AZ, UK

^c Université Sorbonne Paris Nord, Laboratoire des Sciences des Procédés et des Matériaux, LSPM, CNRS, UPR 3407, F-93430, Villetteuse, France



ARTICLE INFO

Keywords:

Hydrogen embrittlement
Crystal plasticity
Dislocations
Finite element
Failure

ABSTRACT

Understanding of years-old multifaceted hydrogen-assisted damage evolution necessitates efforts to model the coupled diffusion-mechanics response in metallic materials. Informed by the dislocation-hydrogen interactions, understood earlier via experiments and/or multi-scale modeling techniques, this work presents a dislocation density-based crystal plasticity model coupled with a hydrogen diffusion/trapping model to simulate the hydrogen-assisted deformation and failure under the HELP mechanism of hydrogen embrittlement. The important role of hydrogen on dislocation multiplication, annihilation and dislocation interaction weakening are included in the presented framework. Two possible scenarios under HELP mechanism, leading to H-induced macroscopic softening or hardening as a result of trade-off between the hydrogen-induced weakening of dislocation interactions and hydrogen-induced increased dislocation density emerges from the simulation studies. These finding points towards the inevitable role of HELP mechanism to cause early failure in metals either working independently or in support with additional mechanisms.

1. Introduction

Hydrogen-induced premature failure in structural metallic materials is a foremost concern toward the sustainable hydrogen economy. With no common consensus on the dominance of the underlying mechanism, over the past years, multiple mechanisms are projected as viable explanations of hydrogen embrittlement (HE) (Robertson et al., 2015; Dadfarnia et al., 2015a; Lynch, 2019; Guedes et al., 2020). Hydrogen Enhanced Decohesion (HEDE) and Hydrogen Enhanced Localized Plasticity (HELP) are the two most prevalent mechanisms (Gerberich, 2012). As per HEDE, high hydrogen concentration can promote the quasi-brittle cleavage type failure by reducing the cohesive strength at grain/phase boundaries, crack tip, and interfaces (Oriani, 1972). HELP can be summarized as an effect of dislocation-solute interaction to expedite localized plasticity by promoting dislocation activities (Beachem, 1972; Birnbaum and Sofronis, 1994). The multifaceted problem of HE cannot be expounded with one single mechanism, hence it is usually considered as a synergistic effect of more than one mechanism (Djukic et al., 2019). Experimental investigations (Martin et al., 2012, 2019) confirmed the HE by hydrogen-enhanced plasticity-mediated decohesion (HELP-mediated HEDE). In HELP-mediated HEDE, hydrogen-induced accelerated dislocation activities can enhance the local hydrogen concentration leading to decohesion (Djukic et al., 2019; Martin et al., 2012, 2019). Depending upon localized microstructure, solute concentration,

* Corresponding author.

E-mail address: dhiraj.mahajan@iitrpr.ac.in (D.K. Mahajan).

and loading conditions, microscopic softening instigated by hydrogen-defect interaction can result in macroscopic hardening and/or softening (Birnbaum and Sofronis, 1994). To comprehend the complex HE phenomenon, and to understand the exact HE mechanism, it is advisable to interpret the macroscopic deformation behavior in the light of the microscopic bits of evidence i.e. defect concentration and distribution (Martin et al., 2019). Based upon the evidence emanating from experiments (Ferreira et al., 1998; Robertson, 2001; Wang et al., 2013), theoretical calculations (Sofronis, 1995; Delafosse, 2012), and multi-scale simulations (Gu and El-Awady, 2018; Yu et al., 2020a,b), hydrogen-dislocation interaction emerges as the most crucial factor to comprehend the HE response of materials (Robertson et al., 2015).

Hydrogen affects the dislocation nucleation (Stenerud et al., 2017; Barnoush et al., 2012), mobility (Sirois and Birnbaum, 1992; Taketomi et al., 2011), and interaction (Ferreira et al., 1998; Castelluccio et al., 2018; Yu et al., 2019) behavior significantly. Beachem (1972) observed that hydrogen enhances ductility (localized) by unlocking the dislocation (instead of locking) and allows dislocations to multiply and move at lower stress levels. Sirois and Birnbaum (1992) reported a decrease in the activation free enthalpy and the activation free energy of dislocation slip for hydrogenated samples. The reduction in activation free enthalpy and the activation free energy indicates a lesser energy requirement for the movement of dislocations under a hydrogen atmosphere (Wang et al., 2013; Yuan et al., 2020). Nanoindentation studies have reported a decrease in “pop-in” load in the presence of hydrogen and this can be interpreted as a decrease in the load to produce dislocations homogeneously (Stenerud et al., 2017; Barnoush et al., 2012). In-situ transmission electronic microscopy (TEM) investigations conducted under hydrogen atmosphere on a variety of materials ensued an increase in dislocation mobility, decrease in spacing between dislocations and decrease in cross-slip probability (Ferreira et al., 1998). Birnbaum and Sofronis (1994) originated the concept of “hydrogen elastic shielding” which accounts for the HELP mechanism partially. According to this, hydrogen shields the interaction of dislocations with elastic stress centers, consequently yields in reduced spacing in pile-ups while enhancing the mobility of dislocations. Based upon the shielding effect mechanism, Chateau et al. (2002) introduced a ‘screening index’ to capture the relative reduction in pair interactions in the presence of bulk hydrogen. Delafosse (2012) incorporated this screening index in classical expressions of the line energy and line tension to discuss the effect of hydrogen on increased dislocation nucleation, weakening of dislocation junctions, and decrease in cross-slip probability.

Recently, Gu and El-Awady (2018) developed a 3D discrete dislocation dynamics framework and simulated the hydrogen elastic shielding effect similar to the one observed in experimentation but only at high hydrogen concentration. Sills and Cai (2018) introduced the significance of interactions between hydrogen atoms on the dislocation core region as solute–solute interactions alter the dislocation core energy. Yu et al. (2020a,b) performed the discrete dislocation plasticity (DDP) simulations by considering both hydrogen elastic shielding (Gu and El-Awady, 2018) and the effect of hydrogen on the dislocation core energy (Sills and Cai, 2018). Hydrogen was observed to decrease the core energy of dislocations, which reduced the dislocation core force. Authors referred to this as “hydrogen core force shielding”. Similar to the “hydrogen elastic shielding”, “hydrogen core force shielding” resulted in enhanced dislocation generation, reduction in flow stress of dislocations, and reduced spacing in pile-ups but at much lower hydrogen concentration realistic for FCC and BCC metals (Yu et al., 2020a,b). The authors observed clear supremacy of hydrogen core force shielding, whereas the contribution of hydrogen elastic shielding was negligible at realistic (low) hydrogen concentrations. Informed by atomistic data, these DDP simulations (Gu and El-Awady, 2018; Yu et al., 2020a,b) complement the experimental evidence of increased dislocation density along with a decrease in dislocation pile-ups spacing (Ferreira et al., 1998; Girardin et al., 2015; Wang et al., 2017). These small-scale simulations on discrete dislocation level along with experimental knowledge are highly informative. However, the length scale associated with DDP simulations puts a limit on their use to model the synergistic role of various microstructural and external factors affecting hydrogen distribution, segregation, and associated HE mechanisms at a larger scale (Delafosse, 2012; Tarleton, 2019). The length scale associated with the finite element based crystal plasticity (CP) makes it the most promising choice for simulating the interconnection of small-scale phenomena with their macroscopic consequences. Castelluccio et al. (2018) made an initial attempt to model the hydrogen effect on macroscopic response of Nickel (Ni) single crystal by just varying the materials parameters informed by multi-scale simulations. However, their argument of hydrogen-induced hardening in FCC metals by an increase in activation energy was contradicting the experimental observations. Various other researchers (Ilin et al., 2014; Charles et al., 2017, 2019; Hassan et al., 2019; Zirkle et al., 2021; Hussein et al., 2021) used coupled crystal plasticity and hydrogen diffusion/trapping model to study the role of hydrostatic stress, yield strength, hydrogen content and plastic deformation on the distribution of hydrogen in polycrystalline materials. Recently, Kumar and Mahajan (2020) developed a dislocation density-based (one-way) coupled crystal plasticity-hydrogen diffusion/trapping model to simulate the effect of loading conditions on hydrogen distribution in the microstructure. However, during the event of hydrogen embrittlement, while evolution of hydrostatic stress and plastic deformation affects the hydrogen distribution behavior; hydrogen concentration also affects the deformation behavior. Consequently, there is a requirement for a coupled diffusion-mechanics framework capable to simulate the real-time hydrogen distribution and its effect on defects evolution behavior controlling the overall deformation behavior in single crystal and polycrystalline configurations. Summarizing the recent experimental observations conducted to study the hydrogen effect (H-effect) on single crystal with single-slip orientation, single crystal with multiple-slip orientation and polycrystals, following points can be concluded: (a) hydrogen effect depends upon initial crystal orientation (hydrogen resulting stage-II hardening in single-slip orientation (Delafosse, 2012; Girardin et al., 2015) can result softening in the multiple-slip orientation (Ghermaoui et al., 2019)) (b) there is direct correlation between the hydrogen effect on fundamental properties of dislocations and the macroscopic behavior (Girardin et al., 2015; Wang et al., 2017; Ghermaoui et al., 2019), (c) configurations subjected to high degree of multiple-slip i.e. polycrystals and single crystals oriented for multiple-slip exhibits similar H-effect on dislocation structure (Wang et al., 2017; Ghermaoui et al., 2019), (d) for same nominal strain level, hydrogen develops an advanced state of deformation favorable for instigating localized failure (Girardin et al., 2015; Wang et al., 2017), (e) all the above discussed points can be very well explained

by the hydrogen-dislocation interaction under the proposition of HELP mechanism, and lastly, (f) absence of modeling framework capable to predict these experimental observations (a–e) accurately.

Under the impression of above discussion, and motivated by the need, this manuscript presents a predictive coupled diffusion-mechanics framework to simulate the H-effect ranging from single crystal to polycrystalline configurations. Dedicated to simulating the hydrogen assisted deformation and failure behavior emanating from the hydrogen-dislocation interaction under the proposition of HELP mechanism, presented computational framework comprises a dislocation density based crystal plasticity model coupled with a hydrogen diffusion/trapping model to simulate the two-way effect (Bal et al., 2018; Vassios, 2015; Ogosi et al., 2020). In the two-way effect, while hydrostatic stresses and dislocation density is affecting the hydrogen redistribution; hydrogen trapped at the dislocations is affecting the associated critical stresses, interaction strength of dislocations and multiplication/annihilation behavior of dislocations. As advisable (Tarleton, 2019), the framework is calibrated with the micromechanical tests performed on the same materials with and without hydrogen.

The theoretical foundation of the developed two-way diffusion-mechanics framework is detailed in Section 2. Section 3 describes the simulation results obtained for the single crystal and polycrystalline configurations. Obtained results are discussed in Section 4 comparing the macroscopic flow behavior with the microscopic dislocation structures evolution observed experimentally for with and without hydrogen. Results show that the proposed framework is capable to predict the hydrogen-induced modified dislocation structures similar to the one observed in experiments. Hydrogen-induced premature failure emerging from accelerated dislocation activities due to the hydrogen-induced shielding, substantiate the failure caused by the HELP mechanism of hydrogen embrittlement. Section 5 presents the various conclusions drawn from the present work followed by the reference section.

2. Theory

2.1. Hydrogen diffusion/trapping model

Hydrogen dissolved in metallic materials resides at interstitial sites and trap sites denoted as C_L and C_T , respectively. Considering dislocations as the only kind of trapping site in the present work, the total hydrogen trapped by dislocations lying at α slip system is written as C_T^α . Hence, $C_T = \sum_{\alpha=1}^{N_s} C_T^\alpha$ is the total hydrogen concentration trapped by dislocations along all the slip systems at a material point. N_s is the total number of slip systems (here for FCC $N_s=12$). Accordingly, the total hydrogen concentration at a material point is:

$$C_{Tot} = C_L + \sum_{\alpha=1}^{N_s} C_T^\alpha \quad (1)$$

Considering, only C_L as responsible for diffusion, the chemical potential of lattice hydrogen μ_L under the influence of hydrostatic stress (σ_H) is (Li et al., 1966):

$$\mu_L = \mu_L^0 + RT \ln \frac{C_L}{N_L} - V_H \sigma_H \quad (2)$$

where, μ_L^0 is the reference lattice chemical potential, R is the universal gas constant, T is the absolute temperature, N_L is the number of lattice sites and V_H is the partial molar volume of hydrogen in metals. Considering the evolution of total hydrogen concentration in an enclosed volume dV of a metallic microstructure equal to the net hydrogen flux, \mathbf{J} , at the surface with unit normal vector \mathbf{n} , and surface area dS , the mass conservation equation takes the form as,

$$\frac{\partial}{\partial t} \int_V (C_L + \sum_{\alpha=1}^{N_s} C_T^\alpha) dV + \int_S \mathbf{J} \cdot \mathbf{n} dS = 0 \quad (3)$$

The hydrogen flux through the surface can be expressed as,

$$\mathbf{J} = -\frac{D_L C_L}{RT} \nabla \mu_L \quad (4)$$

where, D_L is the diffusion coefficient for hydrogen. On substituting the expression of chemical potential Eq. (2) in Eq. (4), we get

$$\mathbf{J} = -D_L \nabla C_L + \frac{D_L C_L V_H}{RT} \nabla \sigma_H \quad (5)$$

By using Eq. (5) in Eq. (3),

$$\frac{\partial}{\partial t} \int_V (C_L + \sum_{\alpha=1}^{N_s} C_T^\alpha) dV + \int_S (-D_L \nabla C_L + \frac{D_L C_L V_H}{RT} \nabla \sigma_H) \cdot \mathbf{n} dS = 0 \quad (6)$$

Using the divergence theorem, above equation can be rewrite as,

$$\frac{\partial C_L}{\partial t} + \sum_{\alpha=1}^{N_s} \frac{\partial C_T^\alpha}{\partial t} - \nabla \cdot (D_L \nabla C_L) + \nabla \cdot \left(\frac{D_L C_L V_H}{RT} \nabla \sigma_H \right) = 0 \quad (7)$$

Considering the occupancy of hydrogen atoms in lattice sites as θ_L , and the occupancy of hydrogen in dislocations at α slip system as θ_T^α , the hydrogen concentrations in lattice and trap sites can be written as:

$$C_L = \theta_L N_L \quad \& \quad C_T^\alpha = \theta_T^\alpha N_T^\alpha \quad (8)$$

where, N_T^α is the trap density along α slip system. For FCC materials N_T^α is expressed in terms of the total dislocation density ρ^α , as (Dadfarnia et al., 2015b),

$$N_T^\alpha = \frac{\sqrt{3}}{a} \rho^\alpha \frac{1}{N_A} \quad (9)$$

where, a is the lattice parameter, N_A is the Avogadro number. The equilibrium between the occupancy of the hydrogen atoms in lattice and trap sites is given by Oriani (1970). Here, it is assumed that the distribution of hydrogen between the lattice sites and dislocation cores lying along particular slip system could be achieved by using the Oriani equilibrium (Oriani, 1970) as,

$$\frac{\theta_T^\alpha}{(1 - \theta_T^\alpha)} = \frac{\theta_L}{(1 - \theta_L)} \exp(-W_b/RT) \quad (10)$$

where, W_b is the trapped binding energy assumed to be independent of the slip system. Using Eq. (10), the concentration of hydrogen trapped at dislocations along α slip system can be obtained as,

$$C_T^\alpha = \frac{\theta_L N_T^\alpha K_T}{(1 - \theta_L) + K_T \theta_L} \quad (11)$$

where, a constant $K_T = \exp(-W_b/RT)$ is used. Following Krom et al. (1999) and Kumar and Mahajan (2020) the partial derivative of the trap hydrogen concentration with respect to time is defined as,

$$\frac{\partial C_T^\alpha}{\partial t} = \frac{\partial C_T^\alpha}{\partial C_L} \frac{\partial C_L}{\partial t} + \theta_T^\alpha \dot{N}_T^\alpha \quad (12)$$

where, $N_T^\alpha = N_T^\alpha(\rho^\alpha(|\dot{\gamma}^\alpha|))$. The rate of change of N_T^α with plastic flow i.e. with evolution of dislocation density is given as:

$$\dot{N}_T^\alpha = \frac{\partial N_T^\alpha}{\partial \rho^\alpha} \frac{\partial \rho^\alpha}{\partial \dot{\gamma}^\alpha} |\dot{\gamma}^\alpha| \quad (13)$$

Using Eq. (13) in Eq. (12),

$$\frac{\partial C_T^\alpha}{\partial t} = \frac{\partial C_T^\alpha}{\partial C_L} \frac{\partial C_L}{\partial t} + \theta_T^\alpha \frac{\partial N_T^\alpha}{\partial \rho^\alpha} \frac{\partial \rho^\alpha}{\partial \dot{\gamma}^\alpha} |\dot{\gamma}^\alpha| \quad (14)$$

Following Eq. (11) we have,

$$\frac{\partial C_T^\alpha}{\partial C_L} = \frac{K_T N_L N_T^\alpha}{(N_L + (K_T - 1)C_L)^2} \quad (15)$$

Using the aforementioned equations in the mass conservation Eq. (7), a slip rate based hydrogen diffusion/trapping model (an adaptation from Krom et al. (1999)) can be written as,

$$\begin{aligned} & \left(1 + \sum_{\alpha=1}^{N_s} \frac{\partial C_T^\alpha}{\partial C_L} \right) \frac{\partial C_L}{\partial t} - \nabla \cdot (D_L \nabla C_L) + \nabla \cdot \left(\frac{D_L C_L V_H}{RT} \nabla \sigma_H \right) \\ & + \sum_{\alpha=1}^{N_s} \left(\theta_T^\alpha \frac{\partial N_T^\alpha}{\partial \rho^\alpha} \frac{\partial \rho^\alpha}{\partial \dot{\gamma}^\alpha} |\dot{\gamma}^\alpha| \right) = 0 \end{aligned} \quad (16)$$

As perceptible, in the above hydrogen diffusion/trapping model, the calculation of the hydrogen distribution is coupled with the hydrostatic stress and plastic deformation. This model accounts for the continuous evolution of both interstitial lattice sites and trapping site occupancies with plastic deformation and hydrogen diffusion at any given location. The last term in the hydrogen diffusion/trapping model, Eq. (16), is the slip-rate factor (SRF) balancing the total hydrogen concentration $C_{T_{tot}}$ at a given location by facilitating a corresponding reduction in C_L and subsequent rise of C_T due to the increase in trap density during plastic deformation (Kumar and Mahajan, 2020). Note that the dislocations are considered as trapping sites only, H-transport by the dislocations need additional considerations (Dadfarnia et al., 2015b) which are not considered in this work.

2.2. Crystal plasticity model

2.2.1. Kinematics

Following the multiplicative decomposition (Lee and Liu, 1967), the total deformation gradient, \mathbf{F} reads as,

$$\mathbf{F} = \mathbf{F}_e \mathbf{F}_p \quad (17)$$

where \mathbf{F}_p is the lattice-preserving inelastic deformation gradient that maps to the plastic configuration and \mathbf{F}_e is an elastic deformation gradient that maps from the inelastic to the deformed configuration. The velocity gradient, \mathbf{L} can be written as,

$$\mathbf{L} = \mathbf{L}_e + \mathbf{F}_e \mathbf{L}_p \mathbf{F}_e^{-1} \quad (18)$$

where, $\mathbf{L}_e = \dot{\mathbf{F}}_e \mathbf{F}_e^{-1}$ is the elastic distortion-rate tensor and $\mathbf{L}_p = \dot{\mathbf{F}}_p \mathbf{F}_p^{-1}$ is plastic distortion-rate tensor. In the used crystal plasticity framework, the plastic velocity gradient \mathbf{L}_p is composed of slip rates $\dot{\gamma}^\alpha$ on each slip systems as,

$$\mathbf{L}_p = \dot{\mathbf{F}}_p \mathbf{F}_p^{-1} = \sum_{\alpha=1}^N \dot{\gamma}^\alpha \mathbf{s}^\alpha \otimes \mathbf{m}^\alpha \quad (19)$$

where, s^α and m^α are the orthonormal vectors in the direction of slip and normal to slip plane respectively, for α slip system. ' \otimes ', symbolizes the tensorial product. Second Piola Kirchhoff stress, S in the intermediate configuration is given as,

$$S = C : \frac{F_e^T F_e - I}{2} \quad (20)$$

where, C is fourth order anisotropic elastic stiffness tensor and I is an identity tensor. The resolved shear stress along α slip system is determined as,

$$\tau^\alpha = S : s^\alpha \otimes m^\alpha \quad (21)$$

The Cauchy stress, σ in the current configuration is obtained using push forward approach as,

$$\sigma = \det(F_e)^{-1} F_e S F_e^T \quad (22)$$

2.2.2. Flow rule and hardening law for dislocation density-based CP model

The slip-rate $\dot{\gamma}^\alpha$ along α slip system is determined as (Orowan, 1940),

$$\dot{\gamma}^\alpha = \rho^\alpha b v_0 \left| \frac{\tau^\alpha - \zeta_b^\alpha}{\tau_c^\alpha} \right|^n \operatorname{sign}(\tau^\alpha - \zeta_b^\alpha) \quad (23)$$

where, n is strain-rate sensitivity, b is the Burgers vector length and v_0 is reference velocity. ρ^α , τ^α and τ_c^α are the dislocation density, resolved shear stress, and critical resolved shear stress respectively, along α slip system (Engels et al., 2012). ζ_b^α is the back stress on α slip system introduced to account for the kinematic hardening. The evolution of the resolved backstress follows the nonlinear Frederick–Armstrong type hardening as,

$$\dot{\zeta}_b^\alpha = A_1 \dot{\gamma}^\alpha - A_2 |\dot{\gamma}^\alpha| \zeta_b^\alpha \quad (24)$$

where, A_1 and A_2 are material dependent parameters. Also, the accumulated slip on α slip system is defined as $\gamma_{acc}^\alpha = \int_0^t |\dot{\gamma}^\alpha| dt$. Following Mecking and Kocks (1981), the dislocation density on slip system α is considered to emerge from the balance between the dislocation multiplication and annihilation along that slip system, as:

$$\dot{\rho}^\alpha = (k_{multi} \sqrt{\rho^\alpha} - k_{annih} \rho^\alpha) |\dot{\gamma}^\alpha| \quad (25)$$

where, k_{multi} and k_{annih} are the constants related to dislocation multiplication and annihilation, respectively. During deformation, hardening is controlled by evolution of dislocation density and strength of interaction among dislocations on various slip systems. Following the generalized Taylor equation (Franciosi and Zaoui, 1982), critical resolved shear stress is defined as (Bronkhorst et al., 2019),

$$\tau_c^\alpha = \tau_f^\alpha + c_3 \mu b \sqrt{\sum_{\beta=1}^{N_s} \chi_{\alpha\beta} \rho^\beta} \quad (26)$$

where, τ_f^α is the strain independent initial slip resistance on slip system α due to frictional resistance and solute atoms, here assumed to be same on all the slip systems. c_3 is a fitting constant. $\chi_{\alpha\beta}$ is the Taylor co-efficient matrix representing the strength of interactions between various slip systems (Franciosi and Zaoui, 1982). In FCC crystals with 12 slip systems, the $\chi_{\alpha\beta}$ contains 12^2 coefficients that can be reduced to six independent constants using symmetries. These coefficients are associated with six types of interactions in dislocation on various slip systems (see Appendix). Dislocations gliding on parallel slip systems involve the self-interaction (a_0) and coplanar (a_1) interaction coefficients. Remaining four coefficients account for the interactions between non-coplanar slip systems such as Hirth locks (a_2), collinear interactions (a_3), glissile junctions (a_4), and Lomer–Cottrell locks (a_5). Collinear interactions are considered to generate a strong hardening effect due to the partial annihilation of gliding collinear dislocations segments resulting in generation of highly curved dislocations that require a higher stress to recover a flowing state (Devincre et al., 2006).

2.3. Two-way coupling

During the event of hydrogen embrittlement, while stress-state affects the hydrogen redistribution, hydrogen concentration also affects the stress-strain response of materials by altering local deformation behavior. In the proposed crystal plasticity model, dislocation activities govern the overall material deformation response. Solute hydrogen segregated at the core of dislocation alter the dislocation interactions behavior and hence the evolved stress-strain response (Sills and Cai, 2018; Yu et al., 2020a). The occupancy of hydrogen trapped at dislocations ($\theta_T^\alpha = \frac{C_L^\alpha}{N_T^\alpha}$) is assumed as key quantity to capture the effect of hydrogen on dislocation activities. $\theta_T^\alpha = 1$ narrates that all the trap sites at dislocations along α slip system are fully occupied and give an upper bound for the effect of hydrogen on dislocations activities. θ_T^α , derives its value from lattice occupancy (hence from C_L) and trap binding energy of dislocations (W_b). In FCC, commonly reported trap binding energy (W_b) of dislocation is -10 kJ/mol, whereas in BCC it is -50 kJ/mol (Dadfarnia et al., 2015b). Traps with $W_b = -50$ kJ/mol will saturate at lower C_L values whereas traps with $W_b = -10$ kJ/mol saturates at relatively very high C_L . Selection of θ_T^α as coupling factor can relate the HE at relatively low hydrogen concentration in BCC comparison to FCC materials.

Hydrogen induced shielding (elastic shielding (Birnbaum and Sofronis, 1994) and/or core force shielding (Yu et al., 2020a,b)) accounting for the HELP mechanism reduces the critical activation stress of Frank–Read sources and accelerate the expansion of dislocation loops (Gu and El-Awady, 2018; Yu et al., 2020a,b). This constitutes an increase in the dislocation multiplication rate. Also, the hydrogenated materials exhibit slip planarity due to the reduced probability of cross-slip, which inhibits the onset of dynamic recovery (Delafosse, 2012; Wang et al., 2013). Parameter k_{multi} and k_{annih} in dislocation density evolution law (Eq. (25)) denotes the dislocation multiplication and annihilation kinetics, consequently to capture the hydrogen effect on dislocation generation and annihilation rate these parameters are assumed to depend upon θ_T^α . Accordingly, the dislocation evolution law used in current CP model (Eq. (25)) is modified to capture the role of hydrogen on dislocation evolution rate as:

$$\dot{\rho}^\alpha = (k_{multi}^H \sqrt{\rho^\alpha} - k_{annih}^H \rho^\alpha) |\dot{\gamma}^\alpha| \quad (27)$$

with

$$k_{multi}^H = (1 + l_c \theta_T^\alpha) k_{multi} \quad (28)$$

k_{multi}^H , capture the effect of hydrogen on dislocation storage rate per slip system. High value of k_{multi}^H correspond to an increase in dislocation multiplication rate. Accordingly, to capture the increased dislocation generation rate under hydrogen atmosphere constant l_c is assumed to take positive value. On the other hand, k_{annih}^H capture the effect of hydrogen on the annihilation rate as:

$$k_{annih}^H = (1 + k_c \theta_T^\alpha) k_{annih} \quad (29)$$

Small value of k_{annih}^H corresponds to a decrease in annihilation rate. Accordingly, to capture the role of hydrogen toward the decrease in annihilation rate (due to decrease in annihilation distance and stacking fault energy; hence decreases in cross-slip probability under hydrogen) constant k_c is assumed to take a negative value.

Apart from increase in the dislocation density, hydrogen-induced shielding effect toward the weakening of interaction strength of dislocations can be captured by decreasing the coefficients of interaction matrix ($\chi_{\alpha\beta}$) (Tarleton, 2019). Castelluccio et al. (2018) considered the weakening of self-interaction coefficient only to explain hydrogen-induced closed spacing in dislocation pile-ups, whereas Yu et al. (2019) reported the weakening of Lomer junction strength for FCC material under hydrogen atmosphere. Based upon the multiple DDP-based observations, Tarleton (2019) recommended considering the H-effect on the whole interaction matrix. To the best of the authors knowledge, it is still not clear whether hydrogen affects all types of dislocation interactions equally or in different magnitude. To explore the possible H-induced failure scenarios (developed by HELP mechanism alone or in support with additional mechanisms) due the mutual interactions of hydrogen-induced increase in dislocation density along with weakening of dislocation interactions behavior, here we have considered two different situations as:

Case 1- Hydrogen reduces the strength of all types of dislocation interactions equally (Tarleton, 2019). To account the equal effect of hydrogen-induced-weakening of all type dislocation interactions, $\chi_{\alpha\beta}$ in Eq. (26) is replaced with:

$$\chi_{\alpha\beta}^H = (1 + H_c \theta_T^\alpha) \chi_{\alpha\beta} \quad (30)$$

where, H_c is a constant with negative value indicating the hydrogen-induced decrease in interaction strength.

Case 2- Hydrogen reduces the strength of the self-hardening coefficient only (Castelluccio et al., 2018). Accordingly, only coefficient a_0 in $\chi_{\alpha\beta}$ (in this case, rest of the components of $\chi_{\alpha\beta}$ will remain unaffected) is replaced with:

$$a_0^H = (1 + a_c \theta_T^\alpha) a_0 \quad (31)$$

where, a_c is a constant with negative value indicating the hydrogen-induced decrease in interaction strength.

The role of hydrogen on yield strength is quite complicated. Structural materials may exhibit an increase or decrease in yield strength depending upon the propensity of dislocation pinning due to solute drag effect, vacancy-hydrogen complex formation, and surface-damage/blister formation, which further depends upon crystal structure, material purity, test temperature, hydrogen concentration, and strain rate (Liu and Atrens, 2013; Li et al., 2015; Sills and Cai, 2016). To restrict attention only on hydrogen-dislocation interaction accounting for the HELP mechanism, other phenomena such as solute drag and vacancy concentration effect are not considered in this work. However, the effect of hydrogen on yield strength is incorporated by changing, τ_f^α in Eq. (26) to $\tau_f^{\alpha H} = (1 + T_c \theta_T^\alpha) \tau_f^\alpha$. Here, constant T_c assumes sign and value as per effect of hydrogen on yield strength. Note, a linear dependence of the affected parameters (whole interaction matrix or the self-interaction matrix element only, initial slip resistance, dislocation multiplication and annihilation) on hydrogen (by θ_T^α) is assumed as first approximation adapted from the recommendation based upon DDP (Tarleton, 2019) and crystal plasticity simulations (Schebler, 2010; Ogosi et al., 2020).

2.4. Numerical implementation

The proposed modeling framework is implemented using UMAT (User defined Material) and UMATHT (User defined Material for Heat Transfer) subroutines in the commercial finite element solver Abaqus. UMAT is used to solve the dislocation density based crystal plasticity model, whereas UMATHT is used to solve the hydrogen diffusion/trapping equation (following the analogy between heat transfer and diffusion equation exploited in earlier work by Barrera et al. (2016)). To solve the hydrogen diffusion equation in UMATHT, the gradient of hydrostatic stress is calculated using the procedure as in Hassan et al. (2019). The gradient of hydrostatic stress, slip-rates along slip systems, derivatives such as $\frac{\partial N^\alpha}{\partial \rho^\alpha}$ and $\frac{\partial \rho^\alpha}{\partial \gamma^\alpha}$ obtained from the previous converged time increment are then provided to UMATHT to solve the slip-rate based hydrogen diffusion/trapping model and to provide hydrogen distribution in the

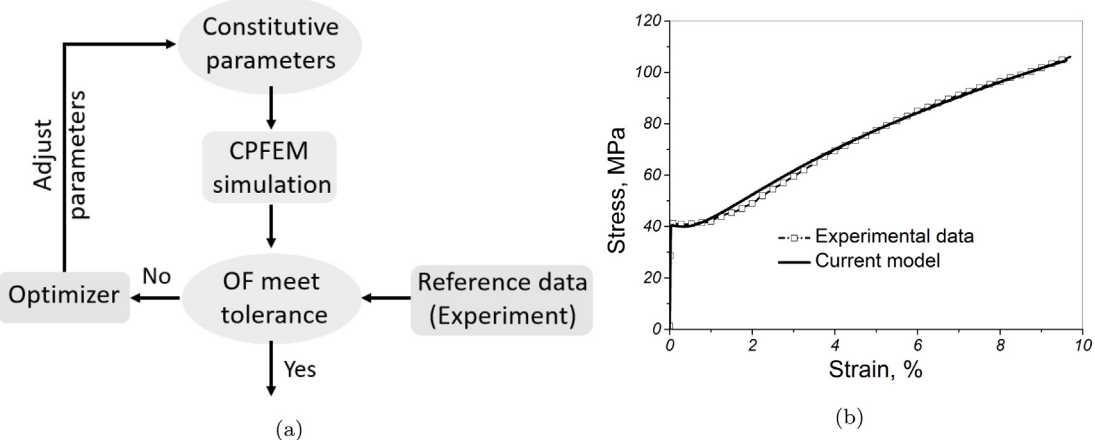


Fig. 1. (a) Schematic of optimization algorithm and (b) stress–strain curve of Ni single crystal with $\langle -167 \rangle$ orientation without hydrogen. Source: Experimental data adapted from Yagodzinsky et al. (2008).

current time increment. To implement two-way coupling scheme for capturing the role of hydrogen on crystal plasticity parameters, θ_T^α from the previously converged time step is provided to the UMAT to solve the mechanical behavior at the current time increment.

The material model presented here is calibrated against the experimental stress–strain curves for Ni single crystal. The parameter identification has been performed using a least square method, using a python script based on the Abaqus 2020 library. This script is directly launched in the CAE console of Abaqus using the SciPy optimization tool (Virtanen et al., 2020) and the Nelder–Mead algorithm which has been shown to be the more efficient for other H-related inverse parameter identification (Delaporte-Mathurin et al., 2021). The implemented optimization strategy performs crystal plasticity finite element simulation(s) and tries to minimize the chosen objective function (OF) by adjusting the parameter space over iterations. In the present work, the deviation between the simulated and experimental single crystal stress–strain data served as the objective function for calibrating the constitutive crystal plasticity parameters. Fig. 1(a) illustrates the general layout of used optimization strategy (see Chakraborty and Eisenlohr (2017) for more details). The optimization algorithm is used in two steps. In the first step, the crystal plasticity parameters are calibrated to replicate the tensile behavior of Ni single crystal without hydrogen. With these calibrated crystal plasticity parameters, in second step hydrogen effect is captured by optimizing the l_c , k_c , H_c or a_c and T_c parameters.

Experimental tensile stress–strain curves of Ni single crystal with $\langle -167 \rangle$ orientation (favor initial single slip system activation) obtained for hydrogen charged and uncharged conditions (see, Figs. 1(b) and 2(a)) from the work of Yagodzinsky et al. (2008) are used as reference data for calibration purpose. Tensile curve for $\langle -167 \rangle$ orientation exhibits stage-I followed by stage-II hardening behavior. Addition of hydrogen results in extension of stage-I with delayed onset of stage-II followed by an increase in stage-II hardening (Yagodzinsky et al., 2008; Delafosse, 2012; Girardin et al., 2015). This complexity in tensile behavior (with and without hydrogen) makes this particular orientation a perfect candidate for good calibration process. However, hydrogen effect depend upon the crystal orientation, also the polycrystalline microstructure favor the high degree of multi-slip systems activation controlling the overall deformation behavior (Wang et al., 2017; Ghermaoui et al., 2019). Consequently, to validate the generality of proposed framework, and to gain a thorough understanding of the hydrogen effect on single crystal to polycrystalline configurations, after validating on single crystal with single-slip configuration, simulations for single crystal with multi-slip orientation and polycrystals were performed.

The single crystal simulations are performed on full dog bone shape tensile specimen (with dimensions of gauge section as $0.3 \times 3 \times 8 \text{ mm}^3$) similar to the one used in experimental work of Yagodzinsky et al. (2008). For polycrystal simulation, an artificial microstructure of size $500 \times 500 \times 5 \mu\text{m}^3$ containing 30 randomly oriented columnar grains obtained from Neper software (Quey et al., 2011) is imported to Abaqus using python scripts (Grilli et al., 2021). For polycrystal, grain boundaries are considered as simply the boundary between two adjacent grains of different orientation (i.e. no special treatment in terms of diffusivity, binding energy, slip transmission, etc. is provided (Kumar and Mahajan, 2020)). C3D8T type elements are used for all types of simulations. All the simulations are performed under uniform strain rate of $9.0 \times 10^{-5} \text{ s}^{-1}$. For simulation under hydrogen atmosphere, all the samples are assumed to be precharged with uniform initial lattice hydrogen concentration. Also, the specimen boundaries are assumed as insulated so that there is no flux of hydrogen away from the specimen.

3. Results

3.1. Tensile behavior of single crystal oriented for single-slip

Inverse identification strategy identified ρ_0 , k_{multi} , and k_{annih} as adjustable parameters to match the simulated stress–strain curve of Ni single crystal oriented for easy glide region with experimental data. Fig. 1(b) presents experimental and simulated uniaxial

Table 1
The crystal plasticity related parameters used in model.

Parameter	Symbol	Magnitude	Units	Reference
Elastic constant	C_{11}	246	GPa	Schebler (2010)
	C_{12}	147	GPa	
	C_{44}	124	GPa	
Inverse strain-rate sensitivity	n	20	–	Kumar and Mahajan (2020)
Burgers vector length	b	2.5×10^{-7}	mm	Kumar and Mahajan (2020)
Slip systems	N_s	12	–	
Initial dislocation density	ρ_0	9.3×10^5	mm^{-2}	Calibrated
Reference dislocation velocity	v_0	5	mm s^{-1}	Kumar and Mahajan (2020)
Dislocation multiplication const.	k_{multi}	303503	mm^{-1}	Calibrated
Dislocation annihilation const.	k_{annih}	10	–	Calibrated
Initial slip resistance	τ_f^α	4	MPa	Assumed a priori
Scaling constant	c_3	1.0	–	Assumed a priori
Back stress parameter	A_1	200	–	Assumed a priori
Back stress parameter	A_2	100	–	Assumed a priori
	a_0	0.122	–	
	a_1	0.122	–	
Interaction coefficients	a_2	0.058	–	Kubin et al. (2008)
	a_3	0.658	–	
	a_4	0.137	–	
	a_5	0.122	–	

Table 2
Hydrogen diffusion/trapping model related parameters.

Parameter	Symbol	Magnitude	Units	Reference
Number of lattice sites	N_L	9.14×10^{-4}	mol mm^{-3}	Schebler (2010)
Dislocation binding energy	W_b	-10	kJ mol^{-1}	Angelo et al. (1995)
Initial lattice H concentration	C_{L0}	1.52×10^{-7}	mol mm^{-3}	–
Hydrogen diffusivity	D_L	6.0×10^{-8}	$\text{mm}^2 \text{s}^{-1}$	Li et al. (2017)
Partial molar volume of H	V_H	2000	$\text{mm}^3 \text{mol}^{-1}$	Li et al. (2017)
Temperature	T	300	K	–
Lattice parameter	a	3.52×10^{-7}	mm	–
Gas constant	R	8314	$\text{N mm mol}^{-1} \text{K}^{-1}$	–

Table 3
Hydrogen fitting constants.

Model type	l_c	k_c	H_c or a_c	T_c
Case 1	47.0	-89.0	-91.0 (H_c)	528.0
Case 2	15.0	-55.0	-75.0 (a_c)	185.0

tensile curves obtained after optimization for Ni single crystal (without hydrogen) with tensile axis aligned with $\langle -167 \rangle$ orientation. A good agreement between the experimental and simulated stress-strain curves in terms of yield stress and hardening behavior shows a successful calibration of the CP model parameters. Proposed model replicates the typical stage I and stage II deformation behavior for $\langle -167 \rangle$ orientation (Yagodzinsky et al., 2008). Table 1 presents the values of constitutive as well as calibrated CP parameters. Table 2 presents the value of parameters used in hydrogen diffusion/trapping model. After optimizing the CP parameters for uncharged condition, inverse optimization was applied to identify l_c , k_c , H_c or a_c and T_c parameters to replicate hydrogen effect on stress-strain curve. Two different sets of values for these constants obtained for Case 1 and Case 2 are shown in Table 3.

Fig. 2(a) presents the simulated tensile stress-strain curves obtained with calibrated parameters for hydrogen charged and uncharged conditions. Under hydrogen charged conditions, Case 1 and Case 2 resulted in the same tensile curve as they are calibrated against the same experimental data. Hydrogen induced increase in yield strength, delay in onset of stage II, and increase in stage II hardening are replicated. Consistent with the Schmid factor calculations, slip system B4 (refer to Appendix for used Schmid and Boas notation of slip systems) dominated as the primary slip system for hydrogen charged and uncharged conditions. This was followed by the activation of A3 as the next dominated slip system during tensile deformation under all the conditions. Contribution from the rest of the slip systems was relatively insignificant, hence, not discussed further.

In contrast to uncharged specimen, both cases under hydrogen charged condition resulted in an increased accumulated slip on the primary slip system (B4), while accumulated slip decreased on the secondary slip system (A3) (see Fig. 2(b)). More localized slip on the primary slip system in Case 2 than in Case 1 (as shown in Fig. 2(b)) is due to the difference in calibration parameters used for both the cases under hydrogen conditions. Fig. 3 presents the dislocation density for hydrogen charged and uncharged conditions. Hydrogen charging increased the total dislocation density for both the cases considered here. However, hydrogen increased the dislocation density on the primary slip system while it decreased on the secondary slip system. Fig. 3 signifies that enhanced total dislocation density under hydrogen arises from the increase in dislocation density on the primary slip system. Hydrogen-induced slip localization with an increase in dislocation density on a particular slip system is considered to emerge as closely spaced

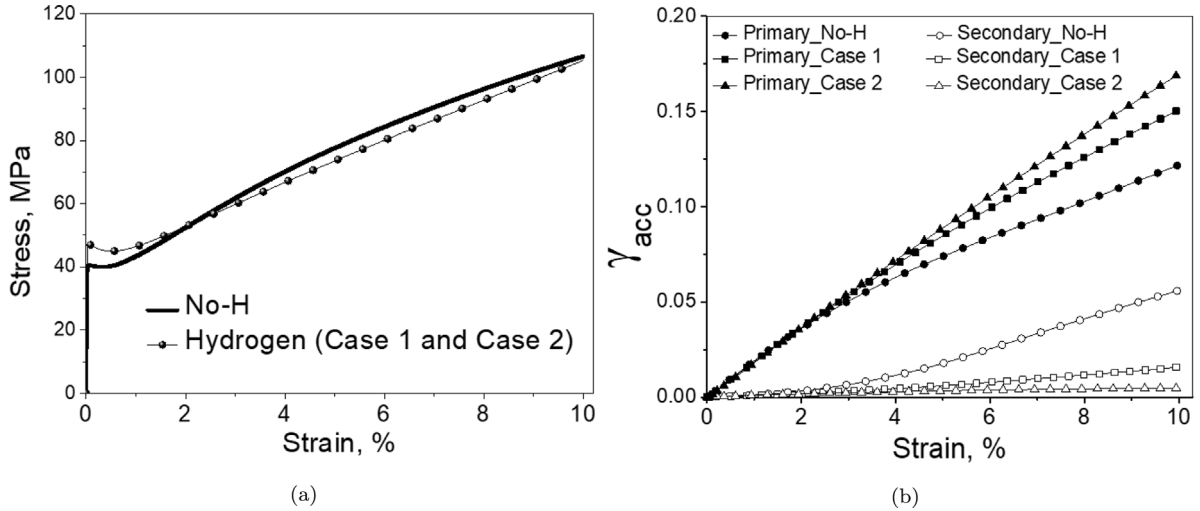


Fig. 2. Simulated (a) stress–strain curves and (b) accumulated slip evolution on primary and secondary slip systems for single crystal with $\langle -167 \rangle$ orientation without and with hydrogen (Case 1 and Case 2).

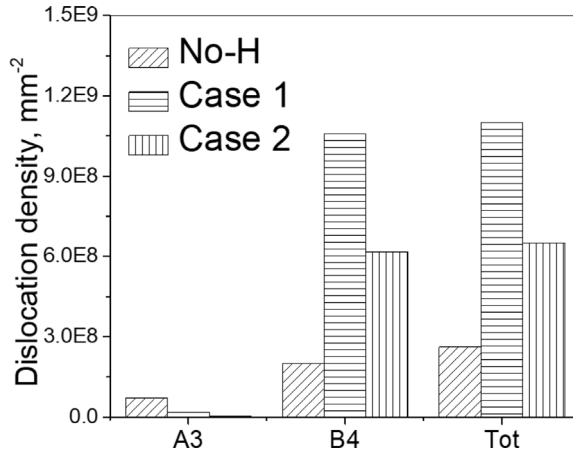


Fig. 3. Dislocation density on primary slip system (B4), secondary slip system (A3), and total dislocation density at the end of deformation for single crystal with $\langle -167 \rangle$ orientation without and with hydrogen (Case 1 and Case 2).

dislocations with planar structure. Under hydrogen charged conditions, Case 1 experience a strong softening effect due to hydrogen induced weakening of all type of dislocation interactions, whereas softening effect is moderate in Case 2 as only self-hardening is compromised. Hence, to exhibit the same tensile flow curve in both cases, Case 1 exhibits higher dislocation density than Case 2 (see Fig. 3).

3.2. Tensile behavior of single crystal oriented for multi-slip

CP and hydrogen related parameters calibrated for single-slip orientation are also applied to simulate the effect of hydrogen on a single crystal with multi-slip orientation $\langle 001 \rangle$. Fig. 4(a) presents the tensile stress–strain curve without and with hydrogen for this orientation. Uncharged sample exhibited the absence of stage I and linear hardening in stage II (typical for multi-slip orientation) with overall tensile flow behavior in close approximation to experimental results (Lawrence et al., 2017; Ghermaoui et al., 2019). Hydrogen addition exhibited an increase in yield strength followed by two extreme conditions of macroscopic softening (for Case 1) and hardening (for Case 2) in reference to the uncharged conditions. Fig. 4(b) presents the total dislocation density evolution in uncharged and hydrogen charged samples for $\langle 001 \rangle$ orientation. As also observed for $\langle -167 \rangle$ orientation, in $\langle 001 \rangle$ orientation hydrogen charging increased the total dislocation density for both Case 1 and Case 2. Case 1, however, exhibited a high dislocation density in comparison to Case 2. Despite the high evolution rate of dislocation density, Case 1 exhibit low hardening rate than Case 2. In multi-slip orientation, all type of dislocation interactions in $\chi_{\alpha\beta}$ contribute to the hardening rate significantly. In Case 1, hydrogen weakens all type of dislocation interactions; whereas in Case 2, only self-hardening is compromised due to hydrogen with

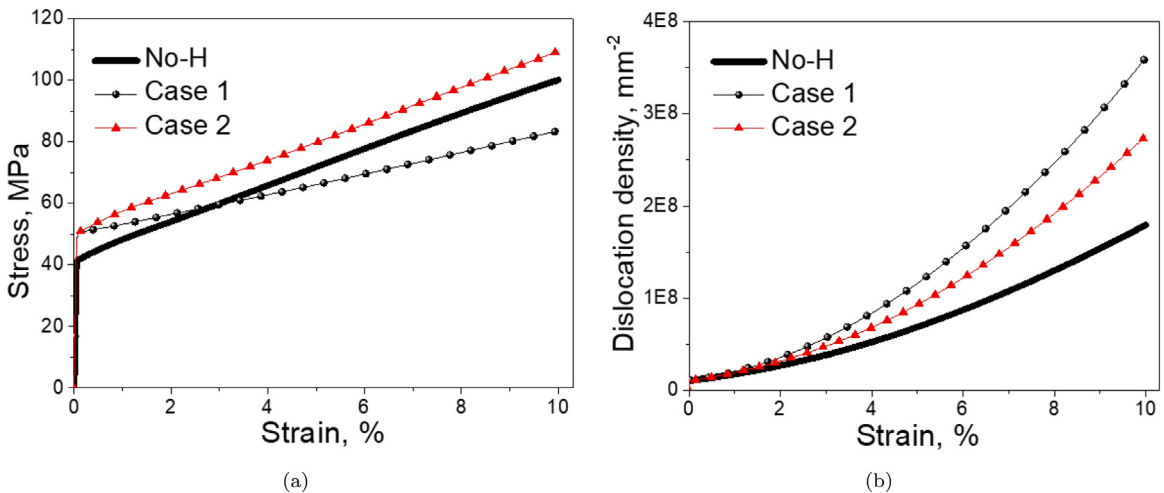


Fig. 4. Simulated (a) stress-strain curve and (b) total dislocation density evolution of single crystal oriented for multi-slip without and with hydrogen (Case 1 and Case 2).

no effect on rest of dislocation interactions type. Consequently, in Case 1 strong effect of hydrogen-induced-weakening of dislocation interactions is dominating the increased hardening rate due to an increase in dislocation density. On the contrary in Case 2, since only the self-hardening component is getting affected, a moderate softening effect is dominated by the hardening effect of hydrogen-induced increase in dislocation density. In view of these observations, comparison of tensile curve behavior specific to Case 1 of single-slip and multi-slip orientation indicates that simulated same HE mechanism that yields hardening at single-slip dominated orientation can cause softening in another (multi-slip) orientation.

Specific to the investigated multi-slip orientation, total eight slip systems (A2, A3, B2, B4, C1, C3, D1, D4) with same Schmid factor got activated. During the course of deformation, activated slip systems exhibited an insignificant difference in the evolution of accumulated slip for uncharged and both hydrogen charged cases (not shown here). Moreover, hydrogen (for both the cases) increased the dislocation density on all the activated slip systems, unlike in the single-slip orientation where dislocation density increased on one of the slip system (primary slip system) while decreased on the other (secondary) slip system. An insignificant difference in the slip accumulation behavior on the activated slip systems for uncharged and hydrogen charged cases corresponds to the experimental observation that hydrogen does not alter the formation process of dislocation structures for this multi-slip orientation (Ghermaoui et al., 2019). Moreover, using the similitude concept (Wang et al., 2017), an increase in dislocation density can be linked with relatively small cell size observed experimentally for multi-slip dominating configurations. Lawrence et al. (2017) reported hydrogen induced increase in yield strength and hardening rate (as observed for Case 2). In contradiction to Lawrence et al. (2017), with nearly similar hydrogen concentration Ghermaoui et al. (2019) reported hydrogen induced increase in yield strength followed by decrease in hardening rate (as observed for Case 1). Moreover, Ghermaoui et al. (2019) reported hydrogen-induced decrease in dislocation cell size but with decreased dislocation density, which contradicts the increase in dislocation density simulated for Case 1. The disparity between the experimental results of Lawrence et al. (2017) and Ghermaoui et al. (2019) along with the observed disparity for simulated dislocation density for Case 1 with experimental observation put forward the need of investigating other factors such as role of hydrogen on vacancy formation, interaction of dislocations with vacancy-hydrogen complexes which otherwise is not in the scope of present work.

3.3. Tensile behavior of polycrystal

In polycrystalline microstructure, grain level elastic and plastic anisotropy results in a variation of stress-strain distribution throughout the microstructure. During deformation, while the evolution of hydrostatic stress and plastic deformation are affecting the hydrogen distribution; hydrogen concentration is also affecting the deformation behavior. Unlike the case of single crystals with nearly homogeneous hydrostatic stress distributions, polycrystals exhibit significant variation in hydrostatic stress as well as in plastic deformation. To simulate the effect of hydrogen on multigrain systems, an artificial polycrystal with randomly oriented grains is generated (see Section 2 for detailed procedure). Fig. 5(a) presents the initial microstructure containing 30 columnar grains with random crystallographic orientation (inverse pole figure (IPF) key in Fig. 5(b)). The simulation model for the polycrystal after meshing in Abaqus is shown in Fig. 5(c). Polycrystal models are subjected to displacement controlled uniaxial tension in the Y-direction using periodic boundary conditions along all directions.

Fig. 6 presents the evolution of hydrostatic stress, lattice hydrogen concentration, trap hydrogen concentration, and total hydrogen concentration in microstructure at the end of deformation. Fig. 6(a, d, g and j) presents the results of one-way coupling only i.e. deformation can alter the hydrogen distribution but hydrogen concentration has no effect on the stress-strain behavior. Figs. 6(b, e, h, k) and 6(c, f, i, l) present the results of two-way coupling for the Case 1 and Case 2, respectively. Significant effect of hydrostatic

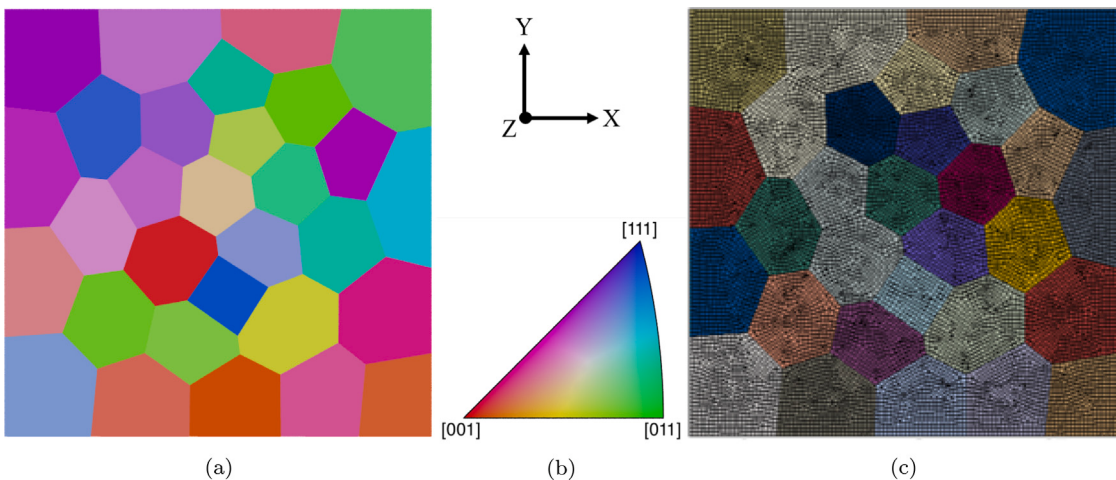


Fig. 5. (a) Polycrystal with randomly oriented grains generated with Neper, (b) inverse pole figure (IPF) key for the grains in figure (a), and (c) finite element mesh obtained from Abaqus.

stress distribution on the evolution of lattice hydrogen concentration is evident from Fig. 6(a–f). Lattice hydrogen is diffusing from the low hydrostatic stress to the high hydrostatic stress region as also reported earlier (Hassan et al., 2019; Hussein et al., 2021). Initial hydrogen concentration, trap concentration (dislocation density) and the associated trap binding energy considered for the current material system resulted in trapped hydrogen concentration almost two orders lower than the lattice hydrogen concentration. Consequently, the distribution of total hydrogen concentration is dominated by the lattice hydrogen concentration (see Fig. 6(j–l)) with the trivial effect of trap hydrogen concentration. This observation is similar to the already reported results by Ilin et al. (2014) and Hussein et al. (2021). As a result of these observations specific to the current material system, hydrostatic stress gradient is concluded as dominating factor to control hydrogen concentration distribution.

Different crystal orientation of the adjacent grains experience different hydrostatic stress across the grain boundaries. High heterogeneity in σ_H at the grain boundaries resulted in local high C_L (and hence $C_{T\sigma_i}$) near the grain boundaries and triple junctions. Relatively high hydrostatic stress gradient resulted in a comparatively high gradient in C_L throughout the polycrystal for Case 2 than the other two cases. Fig. 7 present the contour plots of total dislocation density for hydrogen charged and uncharged conditions. Trapped hydrogen gets accumulated at the regions of high dislocation density (see Figs. 6(g–i) and 7). Hydrogen charging increased the dislocation density as well as fortified heterogeneity in the distribution for both Case 1 and Case 2. However, Case 1 resulted relatively high dislocation density, subsequently higher values of C_T than one-way model and Case 2 (see Fig. 6(g–i)).

Fig. 8(a and b) presents the stress-strain curves and corresponding total dislocation density evolution obtained for one-way, Case 1 and Case 2. In comparison to the one-way model, polycrystal exhibited the hydrogen induced macroscopic softening and hardening for Case 1 and Case 2, respectively. Each randomly oriented grain in polycrystal experiences a different number of active slip systems with significant role of all types of dislocation interactions during deformation. In Case 1, hydrogen reduces the strength of all types of dislocation interactions resulting in a strong softening effect, whereas in Case 2 only self-hardening is reduced by hydrogen resulting in a moderate softening effect. Consequently, for Case 1 even if the dislocation density is high but the softening effect is dominating and resulting in overall macroscopic softening after hydrogen charging. However, for Case 2, the moderate softening effect is dominated by the dislocation density induced hardening (even the dislocation density is lower than Case 1) and hence resulted in macroscopic hardening (see Fig. 8a for tensile curves). These results highlight the important role of hydrogen on macroscopically observed softening or hardening emerging from the trade-off between the hydrogen-induced microscopic softening (emerging from weak dislocation interactions and decreased stress to bow out the dislocation under the hydrogen atmosphere) and defect concentration induced hardening effect.

Fig. 9 presents the contour plots of von Mises stress distribution in polycrystal under different conditions. Case 2 developed concentrated stress spots in comparison to the one-way model and Case 1. These concentrated stress spots developed near/at the grain boundaries and triple junctions (see Fig. 9(c)) correspond to the location of hydrogen induced high dislocation density (see Fig. 7(c)). Subjected to the stress elevation beyond a critical value at these locations, a stress-controlled premature brittle inter-granular failure can be triggered. Hence, Case 2 can be seen as one of the possible scenarios developed by the HELP mechanism to cause brittle inter-granular failure (Yu et al., 2020a). Absence of intense stress spots in Case 1 even with very high dislocation density as shown in Fig. 9(b) is attributed to the dominating role of hydrogen-induced weakening in dislocation interactions as discussed earlier.

4. Discussion

For uncharged conditions, FCC single crystals oriented for initially single-slip develop the dislocation pattern comprising geometric necessary boundaries (GNBs) and equiaxed dislocation cells between these walls (Girardin et al., 2015). However,

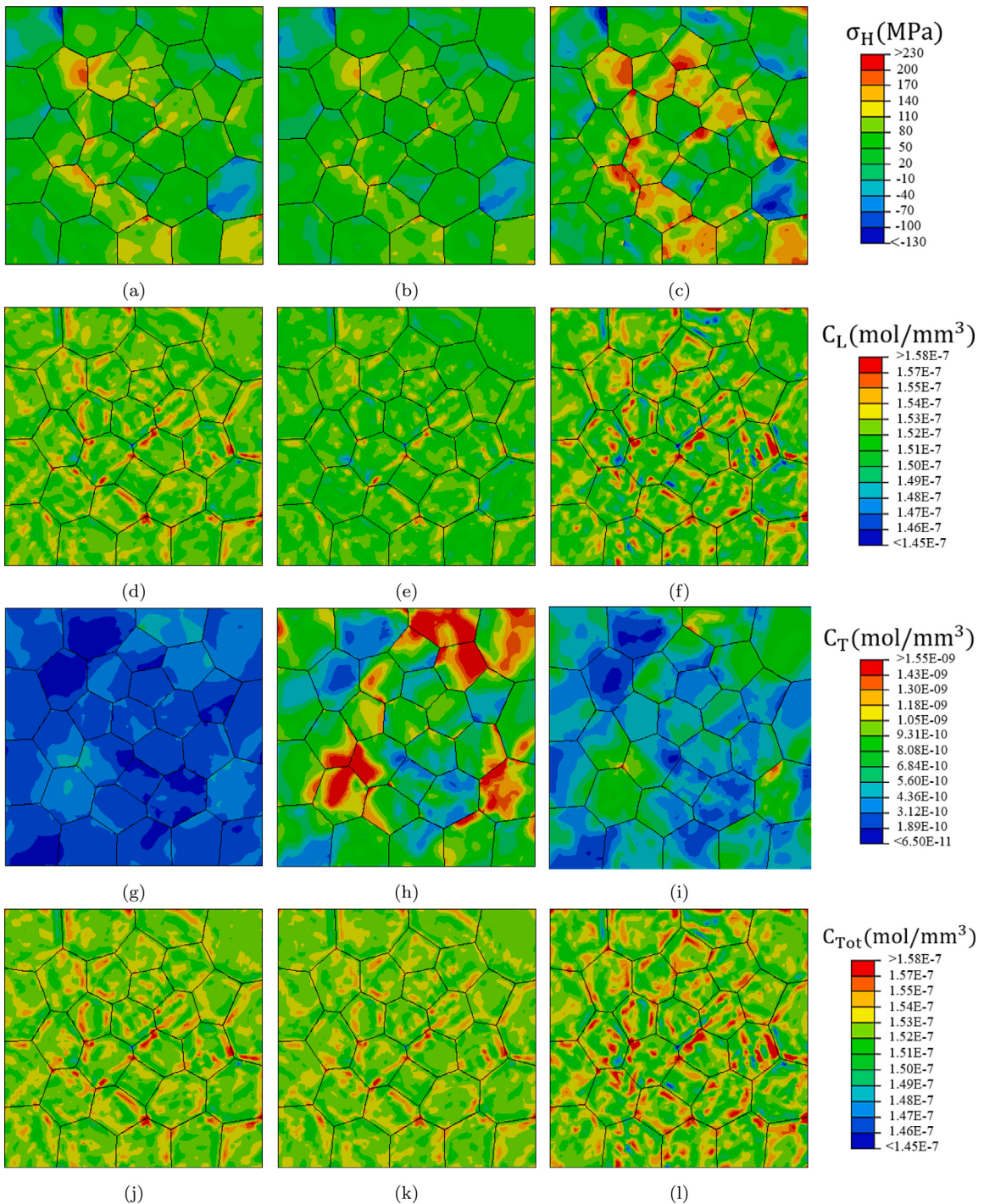


Fig. 6. The evolution of (a–c) hydrostatic stress (σ_H) (d–f) lattice hydrogen (C_L) (g–i) trapped hydrogen (C_T) and (j–l) total hydrogen concentration (C_{Tot}) at the end of deformation. Figures (a, d, g, j) presents the results obtained using the one-way coupling, (b, e, h, k) and (c, f, i, l) of two-way coupling model for Case 1 and Case 2, respectively.

the high degree of multiple-slip for single-crystal with tensile axis oriented for multi-slip and polycrystals develop dislocation pattern comprising mainly the well-defined equiaxed cells where the boundaries of these equiaxed cells are referred to as incidental dislocation boundaries (IDBs) (Wang et al., 2017; Ghermaoui et al., 2019). Recent TEM observations (Girardin et al., 2015; Wang et al., 2017; Ghermaoui et al., 2019) conducted for the same nominal strain demonstrated the effect of hydrogen

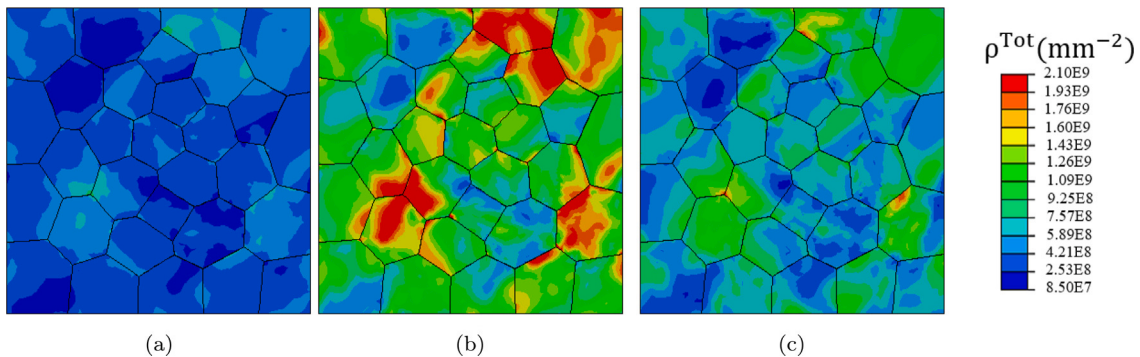


Fig. 7. Evolution of total dislocation density at the end of deformation for (a) one-way model, (b) Case 1, and (c) Case 2 of two-way coupling model.

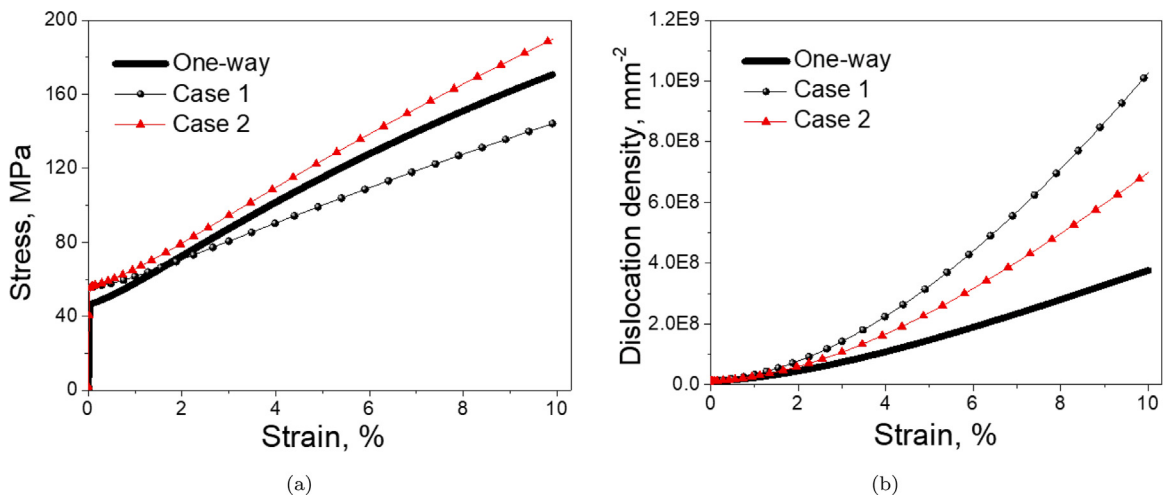


Fig. 8. (a) Tensile stress-strain curve and (b) total dislocation density evolution for polycrystal under various conditions.

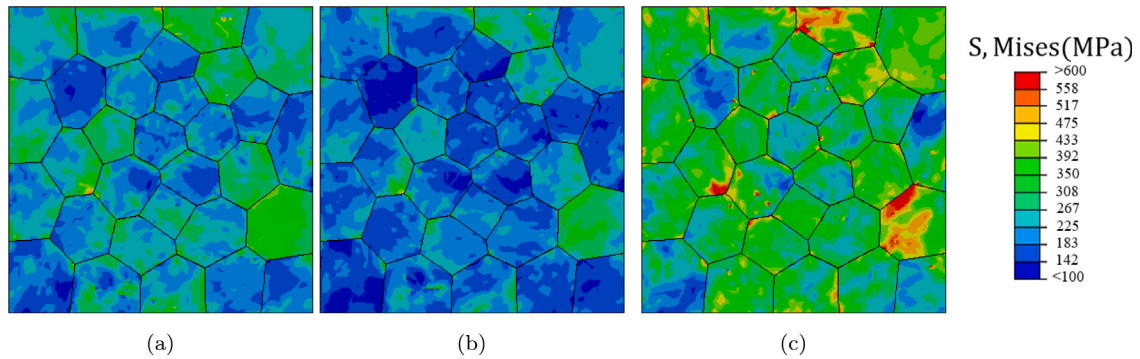


Fig. 9. Evolution of von Mises stress at the end of deformation for (a) one-way model, (b) Case 1, and (c) Case 2 of two-way coupling model.

addition on the dislocation structure evolution. Presence of hydrogen promoted the planar GNBs with reduced spacing for single crystal oriented for single-slip (Girardin et al., 2015). However for polycrystals (Wang et al., 2017) and single crystal oriented for multiple-slip (Ghermaoui et al., 2019), hydrogen is observed to accelerate the evolution of dislocation structures without modifying the dislocation structures formation process (appears as comparatively refined dislocation cells with dense dislocation walls after hydrogen). The simulation results specific to single crystal oriented for initially single-slip predicted hydrogen-induced closely spaced planar dislocation structure. These closely spaced planar dislocation structures i.e. pile-ups formed during an early stage of deformation under hydrogen atmosphere are considered to evolve as planar GNBs with reduced spacing during large deformations (Girardin et al., 2015). Furthermore, these GNBs act as a screen to the dislocation motion and increase the hardening

rate further as observed by Girardin et al. (2015). In contrast to single-slip orientation, simulation results for multi-slip orientation revealed insignificant difference in the slip accumulation behavior for uncharged and hydrogen charged cases that can be associated with the experimental observation (Ghermaoui et al., 2019) that hydrogen does not alter the formation process of dislocation structures for this multi-slip orientation. These observations reveal the crystallographic orientation dependent hydrogen effect on dislocation pattern evolution, which controls the hardening behavior. In polycrystals, Wang et al. (2017) reported a smaller dislocation cells size with dense dislocation walls for Ni material deformed for high-pressure torsion under a hydrogen atmosphere. This observed dislocation structure was attributed to hydrogen-induced decrease in dislocation spacing with increased dislocation density under a hydrogen atmosphere. Increase in total dislocation density observed for polycrystalline simulation under hydrogen atmosphere can be associated with the experimentally observed hydrogen induced decreased cell size with higher dislocation density in cell walls (Wang et al., 2017). Moreover, the configurations subjected to high degree of multi-slip (i.e. polycrystal and multi-slip oriented single crystal) exhibited the similar macroscopic softening and hardening for Case 1 and Case 2, respectively. By considering the direct correlation between the hydrogen effect on fundamental properties of dislocations and the macroscopic behavior, it can be concluded that the polycrystals and single crystals oriented for multiple-slip should exhibits similar H-effect on dislocation structure.

Altogether, it can be concluded that the hydrogen develops an advanced state of deformation leading to deformation-induced boundaries (i.e. dislocation cell walls/IDBs and cell block walls/GNBs) with high dislocation density. High dislocation density facilitates the rapid void nucleation and growth along these deformation-induced boundaries at a lower stress level (Sills and Boyce, 2020). Martin et al. (2011) correlated the sub-surface intense and highly localized deformation to the ridges like quasi-cleavage fracture surface arising from the growth and coalescence of voids. Accordingly, the hydrogen induced increase in dislocation density simulated for both Case 1 and Case 2 can be viewed as a proposition of the hydrogen-induced rapid void formation along these deformation-induced boundaries within the framework of the hydrogen-enhanced localized plasticity (HELP) mechanism for hydrogen embrittlement (Martin et al., 2011; Robertson et al., 2015).

Moreover, recent DDP simulations (Yu et al., 2020a) reported that the increased dislocation density piling-up against the obstacles develops concentrated stress zones leading to premature failure around that obstacle. Case 2 (in Fig. 9(c)) replicates one such scenario of developed concentrated stress spots around grain boundaries and triple junctions with elevated stress values under a hydrogen atmosphere. These stress spots are formed due to high dislocation density at those locations (see Figs. 7(c) and 9(c) under hydrogen charged conditions for Case 2). Stress value elevated beyond a critical value is considered to induce a stress driven premature failure around these grain boundaries and triple junctions (Yu et al., 2020a). On the other hand for Case 1, hydrogen induced increased dislocation density but lower stress levels (due to the strong softening effect considered) puts the need for an additional HE mechanism to govern ultimate fracture. Though not investigated here explicitly, high dislocation density implies increased hydrogen transport by mobile dislocations. This mechanism is considered to transport the excess amount of hydrogen toward the grain boundaries and triple junctions leading to decohesion by reducing the grain boundary cohesive energy (HEDE mechanism). Due to relatively high dislocation density, this mechanism might control the final fracture in Case 1 pointing toward the HELP-mediated HEDE mechanism responsible for early failure. These observations can be viewed in light of earlier experimental observations of Martin et al. (2012, 2019) where hydrogen-induced plasticity is established as an essential ingredient toward the hydrogen-induced inter-granular failure either by elevated stress values or by high dislocation density induced excessive hydrogen concentration at grain boundaries leading to decohesion. Depending upon the above discussion it can be concluded that hydrogen presence can result in void induced quasi-cleavage fracture or inter-granular fracture at grain boundaries and triple junctions but under all conditions hydrogen induced acceleration of microstructure emanating from H-dislocation interactions under the HELP mechanism remains an important ingredient. In summary, the presented novel two-way framework helped to understand the hydrogen-dislocation interactions under the HELP mechanism toward accelerating the evolution of the microstructure favorable for rapid void nucleation, stress elevation, and also for providing the local high hydrogen concentrations at obstacles leading to decohesion type (HEDE) mechanism, thus controlling the final failure. In the future, the proposed framework will be coupled with the appropriate damage model to simulate the tie-in between various HE mechanisms governing the overall damage behavior under a hydrogen environment. For such simulation, Case 1 can represent the scenario where hydrogen leads to excessive softening with an increase in dislocation density but requiring additional decohesion (HEDE) mechanism causing early failure. Whereas, Case 2 can represent a scenario causing moderate softening with an increase in dislocation density but sufficient local stress elevation leading to failure at grain boundaries and/or triple junctions.

5. Conclusions

To simulate hydrogen-assisted deformation and failure behavior of metals instigated by the HELP mechanism of HE, a novel two-way computational crystal plasticity framework is developed. Dedicated to simulating the hydrogen-dislocation interaction under the HELP mechanism, the role of hydrogen on dislocation multiplication, annihilation, and dislocation interaction behavior is well included. Simulation results obtained for single and polycrystalline configurations are discussed in terms of experimentally observed macroscopic tensile curves and microscopically observed dislocation structure evolution behavior. Following are the conclusions drawn from the present work:

- For Ni material containing weak dislocation type of traps investigated here, hydrogen distribution is primarily dependent on the hydrostatic stress distribution.
- Early stage deformations simulated in the present work validate the hydrogen-induced modifications in dislocation structures observed experimentally in single crystal and polycrystalline FCC materials.
- HELP mechanism, simulated in this work, induces macroscopic softening and/or hardening as a result of trade-off between the hydrogen-induced weakening of dislocation interactions and hydrogen-induced increased dislocation density pointing towards the role of HELP mechanism alone or additional mechanisms (HEDE) required for causing early failure.

Declaration of competing interest

The authors declare that they have no known competing financial interests or personal relationships that could have appeared to influence the work reported in this paper.

Data availability

Data will be made available on request.

Appendix

Interaction matrix for FCC is given below, where A2, A3, A6, B2, B4, B5, C1, C3, C5, D1, D4, D6 are the considered slip systems as per Schmid and Boas notation. A, B, C and D corresponds to $\langle\bar{1}11\rangle$, $\langle111\rangle$, $\langle\bar{1}\bar{1}1\rangle$, and $\langle\bar{1}\bar{1}\bar{1}\rangle$ slip planes, whereas integers 1 to 6 are representing [011], [01̄1], [101], [101][1̄10] and [110] slip directions, respectively (Franciosi and Zaoui, 1982).

	A2	A3	A6	B2	B4	B5	C1	C3	C5	D1	D4	D6
A2	a_0	a_1	a_1	a_3	a_4	a_4	a_2	a_4	a_5	a_2	a_5	a_4
A3		a_0	a_1	a_4	a_2	a_5	a_4	a_3	a_4	a_5	a_2	a_4
A6			a_0	a_4	a_5	a_2	a_5	a_4	a_2	a_4	a_4	a_3
B2				a_0	a_1	a_1	a_2	a_5	a_4	a_2	a_4	a_5
B4					a_0	a_1	a_5	a_2	a_4	a_4	a_3	a_4
B5						a_0	a_4	a_4	a_3	a_5	a_4	a_2
C1							a_0	a_1	a_1	a_3	a_5	a_4
C3								a_0	a_1	a_4	a_2	a_5
C5									a_0	a_4	a_5	a_2
D1										a_0	a_1	a_1
D4											a_0	a_1
D6												a_0

References

- Angelo, J.E., Moody, N.R., Baskes, M.I., 1995. Trapping of hydrogen to lattice defects in nickel. *Modelling Simulation Mater. Sci. Eng.* 3 (3), 289–307.
- Bal, B., Koyama, M., Canadinc, D., Gerstein, G., Maier, H., Tsuzaki, K., 2018. On the utility of crystal plasticity modeling to uncover the individual roles of microdeformation mechanisms on the work hardening response of Fe-23Mn-0.5 C TWIP steel in the presence of hydrogen. *J. Eng. Mater. Technol.* 140 (3), 031002.
- Barnoush, A., Asgari, M., Johnsen, R., 2012. Resolving the hydrogen effect on dislocation nucleation and mobility by electrochemical nanoindentation. *Scr. Mater.* 66 (6), 414–417.
- Barrera, O., Tarleton, E., Tang, H., Cocks, A., 2016. Modelling the coupling between hydrogen diffusion and the mechanical behaviour of metals. *Comput. Mater. Sci.* 122, 219–228.
- Beachem, C.D., 1972. A new model for hydrogen-assisted cracking (hydrogen “embrittlement”). *Metall. Mater. Trans. B* 3 (2), 441–455.
- Birnbaum, H.K., Sofronis, P., 1994. Hydrogen-enhanced localized plasticity—a mechanism for hydrogen-related fracture. *Mater. Sci. Eng. A* 176 (1–2), 191–202.
- Bronkhorst, C.A., Mayeur, J.R., Livescu, V., Pokharel, R., Brown, D.W., Gray, G.T., 2019. Structural representation of additively manufactured 316L austenitic stainless steel. *Int. J. Plast.* 118, 70–86.
- Castelluccio, G.M., Geller, C.B., McDowell, D.L., 2018. A rationale for modeling hydrogen effects on plastic deformation across scales in FCC metals. *Int. J. Plast.* 111, 72–84.
- Chakraborty, A., Eisenlohr, P., 2017. Evaluation of an inverse methodology for estimating constitutive parameters in face-centered cubic materials from single crystal indentations. *Eur. J. Mech. A Solids* 66, 114–124.
- Charles, Y., Gaspérini, M., Fagnon, N., Ardon, K., Duhamel, A., 2019. Finite element simulation of hydrogen transport during plastic bulging of iron submitted to gaseous hydrogen pressure. *Eng. Fract. Mech.* 218, 106580.
- Charles, Y., Nguyen, H.T., Gaspérini, M., 2017. Comparison of hydrogen transport through pre-deformed synthetic polycrystals and homogeneous samples by finite element analysis. *Int. J. Hydrogen Energy* 42 (31), 20336–20350.
- Chateau, J., Delafosse, D., Magnin, T., 2002. Numerical simulations of hydrogen-dislocation interactions in fcc stainless steels.: part I: hydrogen-dislocation interactions in bulk crystals. *Acta Mater.* 50 (6), 1507–1522.
- Dadfarnia, M., Martin, M.L., Nagao, A., Sofronis, P., Robertson, I.M., 2015b. Modeling hydrogen transport by dislocations. *J. Mech. Phys. Solids* 78, 511–525.
- Dadfarnia, M., Nagao, A., Wang, S., Martin, M.L., Somerday, B.P., Sofronis, P., 2015a. Recent advances on hydrogen embrittlement of structural materials. *Int. J. Fract.* 196 (1), 223–243.
- Delafosse, D., 2012. Hydrogen effects on the plasticity of face centred cubic (fcc) crystals. In: Gangloff, R.P., Somerday, B.P. (Eds.), *Gaseous Hydrogen Embrittlement of Materials in Energy Technologies*. Vol. 1. Woodhead Publishing, pp. 247–285.
- Delaporte-Mathurin, R., Hodille, E.A., Mougenot, J., Charles, Y., Grisolía, C., 2021. Parametric optimisation based on TDS experiments for rapid and efficient identification of hydrogen transport materials properties. *Nucl. Mater. Energy* 27, 100984.
- Devincre, B., Kubin, L., Hoc, T., 2006. Physical analyses of crystal plasticity by DD simulations. *Scr. Mater.* 54 (5), 741–746.
- Djukic, M.B., Bakic, G.M., Zeravcic, V.S., Sedmak, A., Rajcic, B., 2019. The synergistic action and interplay of hydrogen embrittlement mechanisms in steels and iron: Localized plasticity and decohesion. *Eng. Fract. Mech.* 216, 106528.
- Engels, P., Ma, A., Hartmaier, A., 2012. Continuum simulation of the evolution of dislocation densities during nanoindentation. *Int. J. Plast.* 38, 159–169.
- Ferreira, P., Robertson, I., Birnbaum, H., 1998. Hydrogen effects on the interaction between dislocations. *Acta Mater.* 46 (5), 1749–1757.
- Franciosi, P., Zaoui, A., 1982. Multislip in fcc crystals a theoretical approach compared with experimental data. *Acta Metall.* 30 (8), 1627–1637.

- Gerberich, W., 2012. 8 - modeling hydrogen induced damage mechanisms in metals. In: Gangloff, R.P., Somerday, B.P. (Eds.), Gaseous Hydrogen Embrittlement of Materials in Energy Technologies. Vol. 1. Woodhead Publishing, pp. 209–246.
- Ghermaoui, I., Oudriss, A., Metsue, A., Milet, R., Madani, K., Feaugas, X., 2019. Multiscale analysis of hydrogen-induced softening in fcc nickel single crystals oriented for multiple-slips: elastic screening effect. *Sci. Rep.* 9 (1), 1–10.
- Girardin, G., Huvier, C., Delafosse, D., Feaugas, X., 2015. Correlation between dislocation organization and slip bands: TEM and AFM investigations in hydrogen-containing Nickel and Nickel-Chromium. *Acta Mater.* 91, 141–151.
- Grilli, N., Tarleton, E., Cocks, A.C., 2021. Neper2CAE and PyCiGen: Scripts to generate polycrystals and interface elements in abaqus. *SoftwareX* 13, 100651.
- Gu, Y., El-Alawy, J.A., 2018. Quantifying the effect of hydrogen on dislocation dynamics: A three-dimensional discrete dislocation dynamics framework. *J. Mech. Phys. Solids* 112, 491–507.
- Guedes, D., Malheiros, L.C., Oudriss, A., Cohendoz, S., Bouhattate, J., Creus, J., Thébault, F., Piette, M., Feaugas, X., 2020. The role of plasticity and hydrogen flux in the fracture of a tempered martensitic steel: A new design of mechanical test until fracture to separate the influence of mobile from deeply trapped hydrogen. *Acta Mater.* 186, 133–148.
- Hassan, H., Govind, K., Hartmaier, A., 2019. Micromechanical modelling of coupled crystal plasticity and hydrogen diffusion. *Phil. Mag.* 99 (1), 92–115.
- Hussein, A., Krom, A.H., Dey, P., Sunnardianto, G.K., Moulton, O.A., Walters, C.L., 2021. The effect of hydrogen content and yield strength on the distribution of hydrogen in steel: a diffusion coupled micromechanical FEM study. *Acta Mater.* 209, 116799.
- Ilin, D.N., Saintier, N., Olive, J.-M., Abgrall, R., Aubert, I., 2014. Simulation of hydrogen diffusion affected by stress-strain heterogeneity in polycrystalline stainless steel. *Int. J. Hydrogen Energy* 39 (5), 2418–2422.
- Krom, A.H., Koers, R.W., Bakker, A., 1999. Hydrogen transport near a blunting crack tip. *J. Mech. Phys. Solids* 47 (4), 971–992.
- Kubin, L., Devincre, B., Hoc, T., 2008. Modeling dislocation storage rates and mean free paths in face-centered cubic crystals. *Acta Mater.* 56 (20), 6040–6049.
- Kumar, R., Mahajan, D.K., 2020. Hydrogen distribution in metallic polycrystals with deformation. *J. Mech. Phys. Solids* 135, 103776.
- Lawrence, S.K., Yagodzinsky, Y., Hänninen, H., Korhonen, E., Tuomisto, F., Harris, Z.D., Somerday, B.P., 2017. Effects of grain size and deformation temperature on hydrogen-enhanced vacancy formation in Ni alloys. *Acta Mater.* 128, 218–226.
- Lee, E., Liu, D., 1967. Finite-strain elastic-plastic theory with application to plane-wave analysis. *J. Appl. Phys.* 38 (1), 19–27.
- Li, S., Li, Y., Lo, Y.-C., Neeraj, T., Srinivasan, R., Ding, X., Sun, J., Qi, L., Gumbsch, P., Li, J., 2015. The interaction of dislocations and hydrogen-vacancy complexes and its importance for deformation-induced proto nano-voids formation in α -Fe. *Int. J. Plast.* 74, 175–191.
- Li, J., Oriani, R., Darken, L., 1966. The thermodynamics of stressed solids. *Z. Phys. Chem.* 49 (3_5), 271–290.
- Li, J., Oudriss, A., Metsue, A., Bouhattate, J., Feaugas, X., 2017. Anisotropy of hydrogen diffusion in nickel single crystals: the effects of self-stress and hydrogen concentration on diffusion. *Sci. Rep.* 7 (1), 1–9.
- Liu, Q., Atrens, A., 2013. A critical review of the influence of hydrogen on the mechanical properties of medium-strength steels. *Corros. Rev.* 31 (3–6), 85–103.
- Lynch, S., 2019. Discussion of some recent literature on hydrogen-embrittlement mechanisms: addressing common misunderstandings. *Corros. Rev.* 37 (5), 377–395.
- Martin, M.L., Dadfarnia, M., Nagao, A., Wang, S., Sofronis, P., 2019. Enumeration of the hydrogen-enhanced localized plasticity mechanism for hydrogen embrittlement in structural materials. *Acta Mater.* 165, 734–750.
- Martin, M.L., Fenske, J.A., Liu, G.S., Sofronis, P., Robertson, I.M., 2011. On the formation and nature of quasi-cleavage fracture surfaces in hydrogen embrittled steels. *Acta Mater.* 59 (4), 1601–1606.
- Martin, M., Somerday, B., Ritchie, R., Sofronis, P., Robertson, I., 2012. Hydrogen-induced intergranular failure in nickel revisited. *Acta Mater.* 60 (6–7), 2739–2745.
- Mecking, H., Kocks, U., 1981. Kinetics of flow and strain-hardening. *Acta Metall.* 29 (11), 1865–1875.
- Ogosi, E., Siddiqi, A., Asim, U.B., Kartal, M.E., 2020. Crystal plasticity based study to understand the interaction of hydrogen, defects and loading in austenitic stainless-steel single crystals. *Int. J. Hydrogen Energy* 45 (56), 32632–32647.
- Oriani, R.A., 1970. The diffusion and trapping of hydrogen in steel. *Acta Metall.* 18 (1), 147–157.
- Oriani, R., 1972. A mechanistic theory of hydrogen embrittlement of steels. *Ber. Bunsenges. Phys. Chem.* 76 (8), 848–857.
- Orowan, E., 1940. Problems of plastic gliding. *Proc. Phys. Soc. (1926–1948)* 52 (1), 8.
- Quey, R., Dawson, P., Barbe, F., 2011. Large-scale 3D random polycrystals for the finite element method: Generation, meshing and remeshing. *Comput. Methods Appl. Mech. Engrg.* 200 (17–20), 1729–1745.
- Robertson, I., 2001. The effect of hydrogen on dislocation dynamics. *Eng. Fract. Mech.* 68 (6), 671–692.
- Robertson, I.M., Sofronis, P., Nagao, A., Martin, M., Wang, S., Gross, D., Nygren, K., 2015. Hydrogen embrittlement understood. *Metall. Mater. Trans. A* 46 (6), 2323–2341.
- Schebler, G.J., 2010. On the Mechanics of the Hydrogen Interaction with Single Crystal Plasticity. University of Illinois At Urbana-Champaign, Illinois, United States.
- Sills, R.B., Boyce, B., 2020. Void growth by dislocation adsorption. *Mater. Res. Lett.* 8 (3), 103–109.
- Sills, R., Cai, W., 2016. Solute drag on perfect and extended dislocations. *Phil. Mag.* 96 (10), 895–921.
- Sills, R., Cai, W., 2018. Free energy change of a dislocation due to a cottrell atmosphere. *Phil. Mag.* 98 (16), 1491–1510.
- Sirois, E., Birnbaum, H., 1992. Effects of hydrogen and carbon on thermally activated deformation in nickel. *Acta Metall. Mater.* 40 (6), 1377–1385.
- Sofronis, P., 1995. The influence of mobility of dissolved hydrogen on the elastic response of a metal. *J. Mech. Phys. Solids* 43 (9), 1385–1407.
- Stenerud, G., Johnsen, R., Olsen, J.S., He, J., Barnoush, A., 2017. Effect of hydrogen on dislocation nucleation in alloy 718. *Int. J. Hydrogen Energy* 42 (24), 15933–15942.
- Taketomi, S., Matsumoto, R., Miyazaki, N., 2011. Atomistic study of the competitive relationship between edge dislocation motion and hydrogen diffusion in alpha iron. *J. Mater. Res.* 26 (10), 1269–1278.
- Tarleton, E., 2019. Incorporating hydrogen in mesoscale models. *Comput. Mater. Sci.* 163, 282–289.
- Vasios, N., 2015. Crystal Plasticity: A Rate-Independent Constitutive Model. The Effect of Hydrogen Concentration. University of Thessaly, Thessaly, Greece.
- Virtanen, P., Gommers, R., Oliphant, T.E., Haberland, M., Reddy, T., Cournapeau, D., Burovski, E., Peterson, P., Weckesser, W., Bright, J., et al., 2020. SciPy 1.0: fundamental algorithms for scientific computing in python. *Nature Methods* 17 (3), 261–272.
- Wang, S., Hashimoto, N., Ohnuki, S., 2013. Effects of hydrogen on activation volume and density of mobile dislocations in iron-based alloy. *Mater. Sci. Eng. A* 562, 101–108.
- Wang, S., Nagao, A., Edalati, K., Horita, Z., Robertson, I.M., 2017. Influence of hydrogen on dislocation self-organization in Ni. *Acta Mater.* 135, 96–102.
- Yagodzinsky, Y., Saukkonen, T., Hänninen, H., Tuomisto, F., Barannikova, S., Zuev, L., 2008. Effect of hydrogen on plastic strain localization in single crystals of nickel and austenitic stainless steel. In: Somerday, B.P., Sofronis, P., Jones, R.C. (Eds.), Proceedings of the International Hydrogen Conference, Wyoming, USA. pp. 97–104.
- Yu, H., Cocks, A.C., Tarleton, E., 2019. The influence of hydrogen on lomer junctions. *Scr. Mater.* 166, 173–177.
- Yu, H., Cocks, A.C., Tarleton, E., 2020a. Simulating hydrogen in fcc materials with discrete dislocation plasticity. *Int. J. Hydrogen Energy* 45 (28), 14565–14577.
- Yu, H., Katzarov, I.H., Paxton, A.T., Cocks, A.C., Tarleton, E., 2020b. Influence of hydrogen core force shielding on dislocation junctions in iron. *Phys. Rev. Mater.* 4 (3), 033607.
- Yuan, S., Zhu, Y., Huang, M., Liang, S., Li, Z., 2020. Dislocation-density based crystal plasticity model with hydrogen-enhanced localized plasticity in polycrystalline face-centered cubic metals. *Mech. Mater.* 148, 103472.
- Zirkle, T., Costello, L., McDowell, D.L., 2021. Crystal plasticity modeling of hydrogen and hydrogen-related defects in initial yield and plastic flow of single-crystal stainless steel 316L. *Metall. Mater. Trans. A* 52 (9), 3961–3977.